Spectral properties of locally correlated electrons in a Bardeen–Cooper–Schrieffer superconductor

2007 J. Phys.: Condens. Matter 19 486211

(http://iopscience.iop.org/0953-8984/19/48/486211)

IOP PUBLISHING JOURNAL OF PHYSICS: CONDENSED MATTER

J. Phys.: Condens. Matter **19** (2007) 486211 (19pp) doi:10.1088/0953-8984/19/48/486211

Spectral properties of locally correlated electrons in a Bardeen–Cooper–Schrieffer superconductor

J Bauer[1], **A Oguri**[2] **and A C Hewson**[1]

[1] Department of Mathematics, Imperial College, London SW7 2AZ, UK
[2] Department of Material Science, Osaka City University, Sumiyoshi-ku, Osaka 558-8585, Japan

E-mail: j.bauer03@imperial.ac.uk

Received 1 August 2007, in final form 14 October 2007
Published 9 November 2007
Online at stacks.iop.org/JPhysCM/19/486211

Abstract

We present a detailed study of the spectral properties of a locally correlated site embedded in a Bardeen–Cooper–Schrieffer (BCS) superconducting medium. To this end the Anderson impurity model with a superconducting bath is analysed by means of numerical renormalization group calculations. We calculate one-and two-particle dynamic response functions to elucidate the spectral excitations and the nature of the ground state for different parameter regimes with and without particle–hole symmetry. The position and weight of the Andreev bound states is given for all relevant parameters. We present phase diagrams for the different ground state parameter regimes. This work is also relevant for dynamical mean field theory extensions with superconducting symmetry breaking.

(Some figures in this article are in colour only in the electronic version)

1. Introduction

As described by Bardeen, Cooper and Schrieffer (BCS) [1] electrons in condensed matter with an attractive interaction assume a superconducting state below a critical temperature, referred to as the BCS state. In this state electrons with antiparallel spins form singlet bound states ($S = 0$) known as Cooper pairs. This pair formation is a fermionic many-body phenomenon as it relies on the existence of a Fermi surface [2]. A singlet ground state due to many-body effects also occurs in a quite different situation, when a magnetic impurity is embedded in a metallic host [3, 4]. This state, known as a Kondo singlet, occurs because the electrons in the metal at low temperature experience a large effective coupling to the localized impurity spin. As a consequence it is energetically favourable to screen the local moment, resulting in a (Kondo) singlet state ($S = 0$).

The BCS superconductivity and the Kondo effect are important topics in their own right, and have been extensively studied by the condensed matter physics community. The interplay

and competition of these two effects have also attracted a lot of interest because metals with magnetic impurities can be superconducting at low temperatures [5–10]. The problem of dealing with the two effects together is complicated because the magnetic impurities have a disruptive effect on the BCS superconducting state and the Kondo singlet formation leads to a breaking of the Cooper pairs. For a recent review on this topic we refer to [11] and references therein. Here we address a particular aspect of the problem which has not so far received much attention, the effects of the superconductivity on the local spectral properties of the impurity. As in earlier studies, we take the BCS superconductor as a fixed reference system and take as a model for the impurity an interacting Anderson model. We employ the numerical renormalization group method (NRG), which is a reliable approach to calculate low temperature spectral functions.

From earlier studies of this model, we know that if the interaction U at the impurity site is weak, the ground state is dominated by the superconducting behaviour and the singlet is predominantly a superconducting one. However, if there is a strong repulsion at the impurity site, such that single occupation is favoured, we have a situation where a single spin is coupled to the superconducting medium. If the superconducting gap Δ_{sc} is very small then, similar to the case with a normal metallic bath, the ground state is a singlet, more specifically a Kondo singlet. If this gap is increased, however, it is not possible to form a Kondo singlet, due to the lack of states in the vicinity of the Fermi level, and the ground state becomes a doublet ($S = 1/2$), corresponding to an unscreened spin at the impurity site. This ground state transition at zero temperature is an example of a quantum phase transition which occurs for a level crossing that depends on a system parameter [12]. The relevant energy scales for this singlet–doublet transition to occur in the Kondo regime are the Kondo temperature T_K and the superconducting gap Δ_{sc}. The Kondo model [13, 14] as well as the Anderson impurity model [15] with superconducting bath has been studied by NRG. In these works the estimate for the ground state transition is given by $T_K/\Delta_{sc} \simeq 0.3$, i.e. for $T_K/\Delta_{sc} > 0.3$ we have a singlet ground state ($S = 0$) while for $T_K/\Delta_{sc} < 0.3$ the ground state is a doublet. We can also consider the transition for a fixed value of Δ_{sc} and increasing values of the local interaction U. In this case, as U increases in the local moment regime, T_K decreases until the singlet to doublet transition occurs at a critical value $U = U_c$.

Due to the proximity effect there is an induced symmetry breaking on the impurity site. As a consequence localized excited states (LES) inside the superconducting gap can be induced at the impurity site. Such states are well known from superconductor–normal–superconductor (SNS) junctions and are usually called Andreev bound states. For a weak on-site interaction the ground state of the system is usually a superconducting singlet ($S = 0$) and the LES is an $S = 1/2$ excitation. It is found that at the ground state transition the bound state energy of the LES becomes zero as measured from the centre of the gap. This is related to the fact that the level crossing occurs there.

In recent years detailed measurements on quantum dot structures have enabled one to probe strong correlation effects [16, 17]. In these experiments a quantum dot is coupled to two leads, which can be superconducting. In such situations finite voltage induced currents [18–21] and Josephson currents [22], induced by a phase difference, were observed experimentally. For a theoretical description of this situation it is important to characterize the Andreev bound states in the gap accurately. Many of the more recent theoretical papers [23–30], focus on a quantum dot embedded in two superconducting baths with different (complex) superconducting order parameters. These situations with two channels and with Josephson or non-equilibrium currents will, however, not be covered in this paper.

For the analysis presented here, which focuses on the spectral properties of locally correlated electrons in the superconducting bath, we use the NRG approach. We start by

outlining some of the details of the NRG calculation with a superconducting medium in section 2. We also describe an analysis of the Andreev bound states in the gap in terms of renormalized parameters, and discuss the limit of a large gap. In section 3 we present results first for the model with particle–hole symmetry. For low energies within the superconducting gap we calculate the position and weight of the LES and also give the values for the induced anomalous on-site correlation. We also present singlet–doublet ground state phase diagrams for the symmetric and non-symmetric cases. As the study is based on NRG, it is capable of describing the full parameter range from weak to strong coupling reliably. There have been a number of NRG studies of this situation in the past [13–15, 27]. However, the dynamic response functions have not been addressed in a satisfactory way. Here we present a thorough study of ground state and spectral properties, which will also be of interest for cases where the Anderson model is used as an effective impurity model in the dynamical mean field theory (DMFT) framework, e.g., when superconductivity is studied in the attractive Hubbard model.

2. The Anderson impurity model with superconducting medium

In the following we consider the Anderson impurity model (AIM) in the form

$$H = H_d + H_{\rm mix} + H_{\rm sc}. \tag{1}$$

The local part H_d, which describes an impurity or quantum dot, is given as usual by

$$H_d = \sum_\sigma (\varepsilon_d + \tfrac{1}{2}U) c^\dagger_{d,\sigma} c_{d,\sigma} + \tfrac{1}{2}U \left(\sum_\sigma c^\dagger_{d,\sigma} c_{d,\sigma} - 1 \right)^2 \tag{2}$$

with the impurity level ε_d and an on-site interaction with strength U. Also the mixing term has the usual form,

$$H_{\rm mix} = \sum_{k,\sigma} V (c^\dagger_{k,\sigma} c_{d,\sigma} + \text{h.c.}). \tag{3}$$

We define $\Gamma = \pi V^2 \rho_{\rm c}$ as the energy scale for hybridization, where $\rho_{\rm c} = 1/2D$ is the constant band density of states of a flat band without superconducting symmetry breaking. The superconducting medium is given in a BCS mean field form

$$H_{\rm sc} = \sum_{k,\sigma} \varepsilon_k c^\dagger_{k,\sigma} c_{k,\sigma} - \Delta_{\rm sc} \sum_k [c^\dagger_{k,\uparrow} c^\dagger_{-k,\downarrow} + \text{h.c.}], \tag{4}$$

where $\Delta_{\rm sc}$ is the isotropic superconducting gap parameter, which is taken to be real for simplicity. In equation (4) the summations runs over all k in a wide band. Another energy scale $\omega_{\rm D}$, the Debye cut-off in BCS theory, could enter at this stage to restrict the summation. As shown in [13] with a scaling argument, this effect does not alter the results substantially and merely leads to slightly different parameters. The choice here corresponds to $\omega_{\rm D} = D$, which was also assumed in earlier work [13, 15]. In appendix A we derive the equation for the non-interacting local d-site Green's function matrix of the system (A.10).

2.1. The numerical renormalization group (NRG) approach

For the NRG approach we have to derive a discrete form of the Hamiltonian, which can be diagonalized conveniently in a renormalization group scheme descending to lower energies. This is done in an analogous fashion as for a metallic medium described in [31, 32]. Essentially, there are three steps which only affect $H_{\rm mix}$ and $H_{\rm sc}$: (1) mapping to a one-dimensional problem, (2) logarithmic discretization and (3) basis transformation. We obtain

$$H_{\rm mix}/D = \sqrt{\frac{2\Gamma}{\pi D}} \sum_\sigma (f^\dagger_{0\sigma} c_{d,\sigma} + \text{h.c.}), \tag{5}$$

and

$$H_{\rm sc}^N/D = \sum_{\sigma,n=0}^{N} \gamma_{n+1}(f_{n\sigma}^\dagger f_{n+1,\sigma} + \text{h.c.}) - \frac{\Delta_{\rm sc}}{D}\sum_{n=0}^{N}(f_{n\uparrow}^\dagger f_{n,\downarrow}^\dagger + \text{h.c.}), \tag{6}$$

where the parameters γ_n have the usual form [4]. For more details we refer to earlier work [13, 15] and a recent review on the NRG method [33].

The iterative diagonalization scheme is set up in the same way as in the standard NRG case. Due to the anomalous term in the superconducting bath $H_{\rm sc}^N$ the charge Q is not a good quantum number of the system. Thus eigenstates can only be characterized in terms of the spin quantum number S. The coefficients γ_n fall off with n, but the second term in (6) does not. Thus the superconducting gap becomes a dominating energy scale for large n and a relevant perturbation. It does not make sense to continue NRG iterations down to energies much below this scale as there are no continuum states anymore in the gap. Therefore, we stop the NRG procedure at an iteration $N = N_{\rm max}$, such that the typical energy scale $\Lambda^{-(N_{\rm max}-1)/2}$ is not much smaller than the superconducting gap $\Delta_{\rm sc}$. In practice, we chose the minimum for this ratio to be 10^{-3} such that the number of NRG iterations $N_{\rm max}$ is between 20 and 50 depending on the magnitude of the gap. We used $\Lambda = 1.8$ in all cases, keep 800 states per iteration and the A_Λ factor [32] is taken into account in the calculations.

The NRG approach constitutes a reliable non-perturbative scheme to calculate $T = 0$ ground state properties of a local interacting many-body problem. By putting together information obtained from different iterations dynamic response functions can also be obtained [4]. Here we calculate these spectral functions in the approach [34, 35] based on the complete Anders Schiller basis [36]. The Green's function of the interacting problem is given by the Dyson equation (A.12), which involves the self-energy matrix $\underline{\Sigma}(\omega)$. In appendix B we describe how the diagonal part of the self-energy $\Sigma(\omega) = \Sigma_{11}(\omega)$ and the off-diagonal part of the self-energy $\Sigma^{\rm off}(\omega) = \Sigma_{21}(\omega)$ can be calculated from dynamic response functions in the NRG calculation, which is in analogy to the method described in [37].

2.2. The Andreev bound states

The denominator of the d-site Green's function, equation (A.12), can vanish inside the gap $|\omega| < \Delta_{\rm sc}$. As the imaginary part of the self-energy is zero in the gap this leads to excitations with infinite lifetime there. They correspond to the localized excited states (LES) or Andreev bound states. For the non-interacting case they are determined by the equation $D(\omega) = 0$ (cf equation (A.11)),

$$\omega^2 - \varepsilon_d^2 - \Gamma^2 + \frac{2\omega^2\Gamma}{E(\omega)} = 0, \tag{7}$$

where the function $E(\omega)$ is given in equation (A.8). The terms in equation (7) are functions of ω^2, so if $E_{\rm b}^0$ is a solution so is $-E_{\rm b}^0$. In general, in the interacting case we have to analyse the equation

$$\left[\omega - \varepsilon_d + \frac{\omega\Gamma}{E(\omega)} - \Sigma(\omega)\right]\left[\omega + \varepsilon_d + \frac{\omega\Gamma}{E(\omega)} + \Sigma(-\omega)^*\right] - \left[\frac{\Gamma\Delta_{\rm sc}}{E(\omega)} - \Sigma^{\rm off}(\omega)\right]\left[\frac{\Gamma\Delta_{\rm sc}}{E(\omega)} - \Sigma^{\rm off}(-\omega)^*\right] = 0. \tag{8}$$

Once the self-energies are calculated it is possible to solve this equation iteratively. Here, we will develop a simplified description by using a low energy expansion of the self-energy. First recall that in the gap, $|\omega| < \Delta_{\rm sc}$, $\mathrm{Im}\Sigma(\omega) = \mathrm{Im}\Sigma^{\rm off}(\omega) = 0$. We expand the real part of the

diagonal self-energy $\Sigma(\omega)$ to first order around $\omega = 0$, which is motivated by the Fermi liquid expansions for the normal metallic case and justified by the numerical results for the behaviour for low frequency. The off-diagonal self-energy is approximated simply by the real constant $\Sigma^{\rm off}(0)$. This approximation for the self-energy is easy to justify if the gap is small parameter, such that it only covers small values of ω. The main objective is to present a simplified picture for the analysis of the Andreev bound state for the interacting system. We do not expect to be able to describe the system near the quantum phase transition accurately like this, and other limitations will be seen in the results later. Hence, we find instead of (8) the simpler equation

$$\omega^2 - \tilde{\varepsilon}_d^2 - \tilde{\Gamma}^2 - z^2\Sigma^{\rm off}(0)^2 + \frac{2\tilde{\Gamma}[\omega^2 + \Delta_{\rm sc} z\Sigma^{\rm off}(0)]}{E(\omega)} = 0, \tag{9}$$

where renormalized parameters $\tilde{\varepsilon}_d = z[\varepsilon_d + \Sigma(0)]$ and $\tilde{\Gamma} = z\Gamma$ were introduced. As usual $z^{-1} = 1 - \Sigma'(0)$. Renormalized parameters for the analysis of the Andreev bound states were also considered in [25, 38]. The definition here corresponds to the renormalized perturbation theory framework for the AIM introduced in [39]. The form of the equations (7) and (9) is very similar and both can be easily solved numerically to give the bound state solutions $\omega = E_{\rm b}^{\alpha} = \alpha E_{\rm b}$, $\alpha = \pm$. Due to the additional off-diagonal correlations induced by the self-energy term $\Sigma^{\rm off}(0)$, a simple interpretation of the interacting theory based on using renormalized parameters $\tilde{\varepsilon}_d$, $\tilde{\Gamma}$ in equation (7) for the non-interacting theory is, however, not possible.

Based on the same idea we can give approximate expressions for the weights of the bound states $w_{\rm b}^{\alpha}$ by expanding the diagonal part of the Green's function around $\omega = E_{\rm b}^{\alpha}$. We can then write the retarded Green's function in the gap near the bound states $\omega \simeq \pm E_{\rm b}$ as

$$G(\omega) = \frac{w_{\rm b}^{-}}{\omega - E_{\rm b}^{-} + {\rm i}\eta} + \frac{w_{\rm b}^{+}}{\omega - E_{\rm b}^{+} + {\rm i}\eta}. \tag{10}$$

Using the above approximation for the self-energy the weights are found to be

$$w_{\rm b}^{\alpha} = \frac{z}{2} E(E_{\rm b})^2 \frac{E(E_{\rm b})(1 + \alpha\frac{\tilde{\varepsilon}_d}{E_{\rm b}}) + \tilde{\Gamma}}{E(E_{\rm b})^2(E(E_{\rm b}) + 2\tilde{\Gamma}) + \tilde{\Gamma}(E_{\rm b}^2 + \Delta_{\rm sc} z\Sigma^{\rm off}(0))}. \tag{11}$$

In a more sophisticated approximation one could consider an expansion of the self-energies around the bound state energies $E_{\rm b}$ rather than $\omega = 0$. Various things can be inferred from expression (11). First we note that in the particle–hole symmetric case, $\tilde{\varepsilon}_d = 0$, $w_{\rm b}^{+} = w_{\rm b}^{-} = w_{\rm b}$. The weights are proportional to the renormalization factor z. Since z shows a similar behaviour as in the metallic lead case they decrease with increasing interaction U according to (11). One can easily see that for bound state energies close to the gap, $|E_{\rm b}| \to \Delta_{\rm sc}$, the weights go to zero, $w_{\rm b}^{\alpha} \to 0$. One finds [15] that for small $U/\pi\Gamma$ and $\Delta_{\rm sc}/\Gamma \ll 1$ we have $E_{\rm b} \to \Delta_{\rm sc}$, and also for large $U/\pi\Gamma$ the bound state energy is close to the gap. Therefore the overall behaviour for $w_{\rm b}$ is given in such a case by $w_{\rm b} \to 0$ for small U, then an increase with U to a maximum and a decay again for large U (cf figure 3 later). At the ground state transition, where $E_{\rm b} = 0$, the weight shows a discontinuity, and from equation (11) this requires a jump of the self-energy as function of U.

2.3. The limit of large gap

In order to obtain some analytical results it is useful to consider the case where the superconducting gap is a large parameter, $\Delta_{\rm sc} \to \infty$ [25, 28, 30, 40]. Then the problem

essentially reduces to a localized model with an anomalous on-site term which is of the order of the hybridization Γ. We will write it in the form

$$H_d^{\infty} = \sum_{\sigma} \xi_d (c_{d,\sigma}^{\dagger} c_{d,\sigma} - 1) - \Gamma[c_{d,\uparrow}^{\dagger} c_{d,\downarrow}^{\dagger} + \text{h.c.}] + \frac{U}{2}\left(\sum_{\sigma} n_{d,\sigma} - 1\right)^2, \quad (12)$$

where $\xi_d = \varepsilon_d + U/2$. Without interaction this Hamiltonian can be diagonalized by a Bogoliubov transformation and the excitation energies $E_d = \sqrt{\xi_d^2 + \Gamma^2}$ are found, which lie in the gap as $\Gamma \ll \Delta_{\text{sc}}$ as assumed initially. This gives a direct picture of the emergence of the Andreev bound states for large Δ_{sc}.

We can discuss the ground state crossover from the singlet to the doublet state in terms of the single-site Hamiltonian (12). First note that the $S = 1/2$ (doublet) states, $|\uparrow\rangle$ and $|\downarrow\rangle$, are eigenstates of (12) with zero energy. The $S = 0$ singlet states, empty site $|0\rangle$ and doubly occupied site $|\uparrow\downarrow\rangle$, are not eigenstates of (12). However, the linear combinations in the 'BCS form',

$$|\Psi_1\rangle = u_d|0\rangle + v_d|\uparrow\downarrow\rangle, \qquad |\Psi_2\rangle = v_d|0\rangle - u_d|\uparrow\downarrow\rangle, \quad (13)$$

are eigenstates with eigenvalues $E_1 = -E_d + U/2$ and $E_2 = E_d + U/2$, respectively. The coefficients u_d, v_d are given by

$$u_d^2 = \frac{1}{2}\left(1 + \frac{\xi_d}{E_d}\right), \qquad v_d^2 = \frac{1}{2}\left(1 - \frac{\xi_d}{E_d}\right). \quad (14)$$

The ground state is therefore a singlet as long as $E_1 < 0$ and a doublet otherwise. The condition $E_1 = 0$ or

$$\frac{\xi_d^2}{U^2} + \frac{\Gamma^2}{U^2} = \frac{1}{4} \quad (15)$$

defines therefore the phase boundary for the transition. It is a semicircle in the (ξ_d/U)–(Γ/U)-plane with radius $1/2$, which is shown in figure 12 later. How this phase boundary looks like for finite gap Δ_{sc} will be investigated in section 3.2, when we look at the situation away from particle–hole symmetry. In the case of particle–hole symmetry $\xi_d = 0$ and condition (15) reduces to $\Gamma = U/2$.

Having established the formalism and the most important relations we will in the next section present results for spectral behaviour of the symmetric AIM with superconducting bath with a finite gap parameter.

3. Results

In this section we present results for the local spectral properties. The diagonal and off-diagonal Green's functions are calculated within the NRG framework usually from the Lehmann representation,

$$\rho_d(\omega) = \frac{1}{Z}\sum_{m,n} |\langle m|c_d^{\dagger}|n\rangle|^2 \delta[\omega - (E_m - E_n)](\mathrm{e}^{-\beta E_m} + \mathrm{e}^{-\beta E_n}), \quad (16)$$

and similar for the off-diagonal Green's function. As in this procedure the discrete excitations for the spectral peaks in the Green's functions have to be broadened, it is not straight forward like this to obtain the sharp spectral gap at $|\omega| = \Delta_{\text{sc}}$ expected for $T = 0$. As detailed in appendix B, we can, however, determine the self-energy matrix from the one-particle Green's function and the higher F-Green's function (cf equation (B.4)). Then we can use the exact expression for the non-interacting Green's function $\underline{G}_d^0(\omega)$ in equation (A.10), which includes

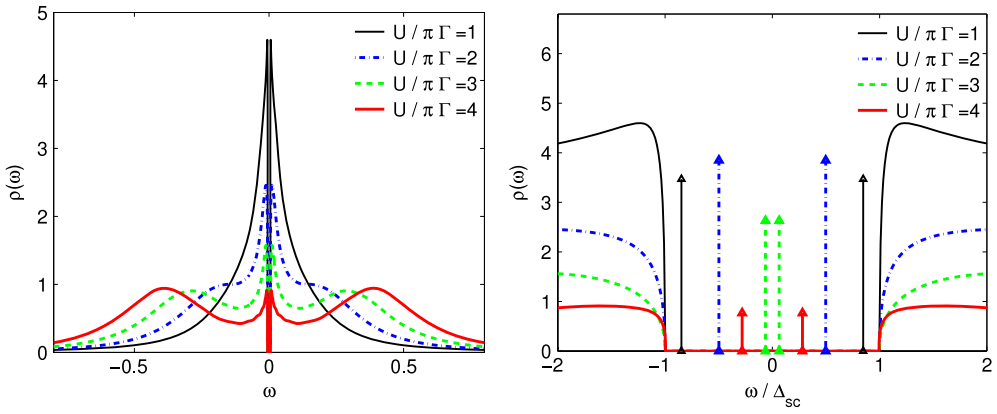

Figure 1. The spectral density $\rho(\omega)$ for various values of U for the whole energy regime (left) and the region in the gap (right); $\Delta_{sc} = 0.005$ and $\pi\Gamma = 0.2$.

a sharp spectral gap, and the Dyson matrix equation (A.12) to calculate the diagonal and off-diagonal Green's function, $G(\omega)$ and $G^{\rm off}(\omega)$ respectively. This is the way the Green's functions are calculated for the region outside the gap, $|\omega| > \Delta_{sc}$. Inside the gap, $|\omega| < \Delta_{sc}$, we have extracted the weights w_b and positions E_b^α of the delta function peaks for the Andreev bound states from the NRG excitation data for the Green's function directly from the lowest spectral excitation (SE) in equation (16). These delta functions are represented by an arrow in the plots. Altogether the diagonal spectral function $\rho(\omega) = -{\rm Im}G(\omega)/\pi$ can then be written in the form

$$\rho(\omega) = \sum_{\alpha=\pm} w_b \delta(\omega - E_b^\alpha) + \rho_{\rm cont}(\omega), \tag{17}$$

where $\rho_{\rm cont}(\omega)$ is the continuum part for $|\omega| > \Delta_{sc}$. The off-diagonal part of the spectrum $\rho^{\rm off}(\omega) = -{\rm Im}G^{\rm off}(\omega)/\pi$ has a general form which is similar to that of the diagonal part,

$$\rho^{\rm off}(\omega) = \sum_{\alpha=\pm} \bar{w}_b^\alpha \delta(\omega - E_b^\alpha) + \rho_{\rm cont}^{\rm off}(\omega), \tag{18}$$

where the weights $\bar{w}_b^\alpha$ can have positive and negative values. For half filling the spectrum $\rho^{\rm off}(\omega)$ is an asymmetric function of ω.

3.1. Symmetric model

We first focus on the particle–hole symmetric model, $\varepsilon_d = -U/2$, where the ratio $U/\pi\Gamma$ and the parameter Δ_{sc} are the relevant energy scales.

3.1.1. Spectral functions for small gap. In figure 1 we show the spectral function (17) for $\Delta_{sc} = 0.005$ for the diagonal Green's function at the impurity site for a number of different values of U. Here and in the following we take a fixed value for the hybridization, $\pi\Gamma = 0.2$. All quantities can be thought of as being scaled by half the band width $D = 1$.

In the plot on the left-hand side we give the spectrum over the full energy range. When the interaction is increased, spectral weight is shifted to higher energies as the atomic limit peaks at $\pm U/2$ develop. We also observe the beginning of the formation of a Kondo resonance at low frequencies. For larger U the Kondo resonance becomes narrower, but its formation is suppressed in the very low frequency regime because the spectral density vanishes in the

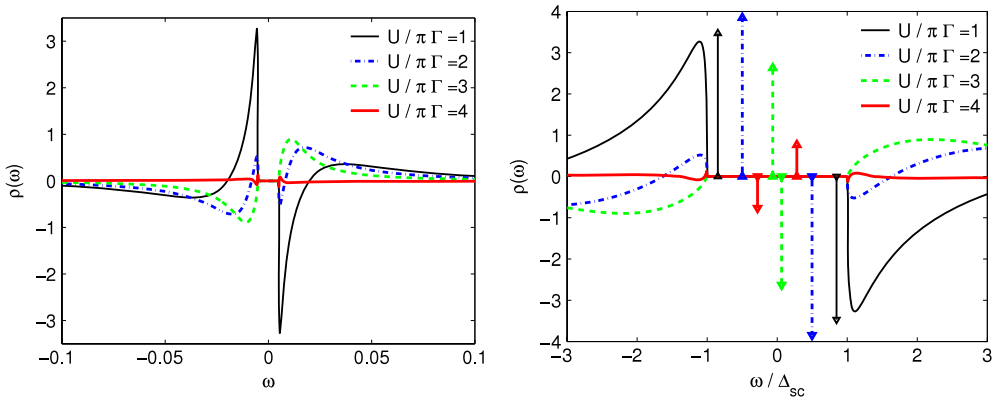

Figure 2. The spectral density $\rho^{\rm off}(\omega)$ for various values of U for the whole energy regime (left) and the region in the gap (right); $\Delta_{\rm sc} = 0.005$ and $\pi\Gamma = 0.2$.

gap region $-\Delta_{\rm sc} < \omega < \Delta_{\rm sc}$. This is not visible on the scale used in the left-hand panel of figure 1. In the right-hand panel of figure 1 we give an enlarged plot of the gap region, which shows the delta function contributions from the Andreev bound states, where the arrows give the position of the bound state $E_{\rm b}^{\pm}$ and their height indicates the spectral weight $w_{\rm b}$. It can be seen that the position of the bound state changes when we increase the interaction. The weight first increases and then decreases as a function of U, which corresponds to the feature which was interpreted earlier using equation (11). It is generally of interest to see how much spectral weight is transferred from the continuum to the bound states, and an overview for this is given in the later figures 8 (right) and 9. Note that the largest value of U shown, is greater than the critical $U_{\rm c}$ for the singlet–doublet transition ($U_{\rm c}/\pi\Gamma \simeq 3.2$). In the high energy spectrum there is no significant change to be seen in the behaviour, however, at low energies we observe the crossing of the bound state energies at $\omega = 0$ at $U_{\rm c}$.

In figure 2 we show the off-diagonal spectral function (18) for $\Delta_{\rm sc} = 0.005$ for a number of different values of U. In the plot on the left-hand side we show the behaviour for the continuum part outside the gap. Notice that the frequency range only extends up to $\omega = \pm 0.1$. We can see a peak close to $\omega = \pm\Delta_{\rm sc}$, which is suppressed for larger U and changes sign towards the singlet–doublet transition. The behaviour of the bound state peaks in the off-diagonal spectrum is displayed on the right-hand side of the figure. We can see similar features as observed before in the diagonal part, i.e. the weight first increases with U and then decreases. If we follow the excitations with the weight of the same sign we can see, that at the singlet–doublet transition the bound state levels cross at $\omega = 0$.

3.1.2. Bound state behaviour. A more detailed analysis of the behaviour of the bound state as a function of $U/\pi\Gamma$ and the gap in the medium $\Delta_{\rm sc}$ is presented in figure 3. On the left-hand side we plot the bound state energies $\pm E_{\rm b}$ and on the right-hand side the corresponding weights $w_{\rm b}$.

We can see that in the non-interacting case the bound state energy for the cases with small gap ($\Delta_{\rm sc} = 0.001, 0.01$) is very close to $\pm\Delta_{\rm sc}$ and decreases to zero with increasing interaction. For a critical value $U_{\rm c}$ the nature of the ground state changes from a singlet ($S = 0$) to a doublet ($S = 1/2$) and at this point $E_{\rm b} = 0$. For this transition we can think of the positive $E_{\rm b}^{+}$ and negative solution $E_{\rm b}^{-}$ for the bound states as crossing at $\omega = 0$. When the interaction is increased further, $\left|E_{\rm b}^{\pm}\right|$ becomes finite again and increases with U. The larger the gap $\Delta_{\rm sc}$ the

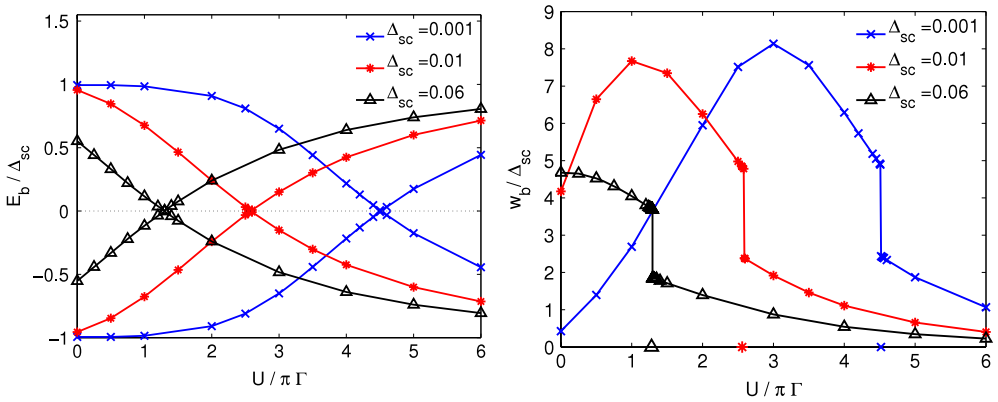

Figure 3. Bound state energies E_b (left) and weights w_b (right) for various $U/\pi\Gamma$ and Δ_{sc}. Both quantities have been scaled by the corresponding value of Δ_{sc}; $\pi\Gamma = 0.2$.

smaller critical value U_c for this ground state transition becomes. In the case where Δ_{sc} is of the order of Γ—as can be seen for the case $\Delta_{sc} = 0.06$—the bound state energy E_b lies in the middle of the gap already for the non-interacting case, but otherwise shows a similar behaviour as described above.

On the right-hand side of figure 3 the weight w_b of these bound states can be seen. We have marked the position U_c of the singlet–doublet crossover point by a symbol on the x-axis. The two curves for a value of the gap $\Delta_{sc} = 0.001$ and $\Delta_{sc} = 0.01$ have a maximum for some intermediate value of U which is smaller than the critical U_c for the ground state transition. This behaviour can be understood from the analytic behaviour of the explicit equation (11) derived earlier. For the other curve ($\Delta_{sc} = 0.06$) the weight is maximal for the non-interacting case. In all cases the weight becomes very small for large U. Note that we plot the weight scaled by the gap parameter, w_b/Δ_{sc}, and therefore the absolute values are larger for the cases with larger superconducting gap. At the singlet–doublet transition we can see discontinuous behaviour as the weight changes sharply. This is a feature of the zero temperature calculation, where the matrix elements in the Lehmann sum (16) change their values discontinuously when the levels cross on increasing U, such that the nature of the ground state changes. It can be seen for the anomalous correlations $\langle d_\uparrow d_\downarrow \rangle$ in figure 8 later, as well. For finite temperature this discontinuity becomes smooth.

3.1.3. Spectral functions for larger gap. In figure 4 we show for comparison the diagonal spectral function for a larger gap $\Delta_{sc} = 0.02$ for the diagonal Green's function at the impurity site for a number of different values of U. The overall picture on the left is similar to the case in figure 1 with the smaller gap. Due to the larger gap the formation of the central Kondo resonance is completely suppressed, but the high energy spectrum is as before. From the behaviour within the gap (right side in figure 4) we can see that the bound state position $E_b^{\pm}$ goes to zero for smaller U values than in the case $\Delta_{sc} = 0.005$, and hence the ground state transition occurs for smaller U_c for the larger gap ($U_c/\pi\Gamma \simeq 2.03$). This was analysed in detail in figure 3. For the values of U shown the spectral weight of the bound states w_b decreases with increasing U. The weight w_b of the peaks in the gap has been scaled differently in figures 1 and 4, so that their height should not be compared directly.

The spectral function of the off-diagonal Green's function at the impurity site (18) for this value of the gap, $\Delta_{sc} = 0.02$, is shown in figure 5 for a number of different values of U.

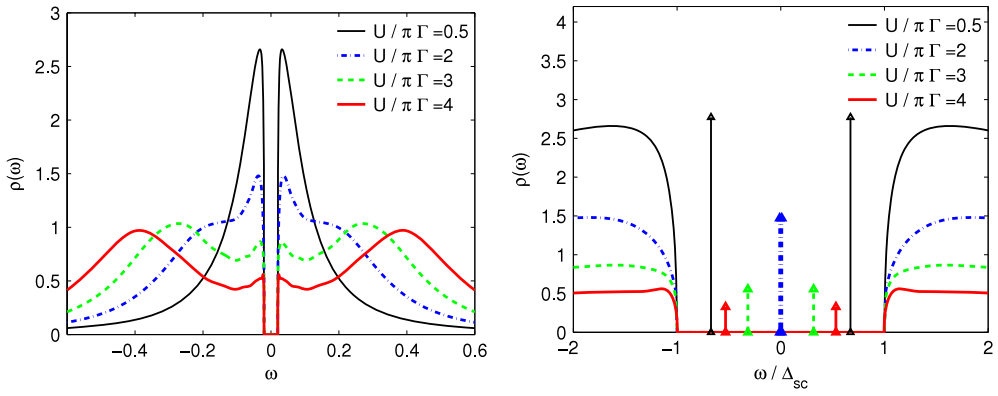

Figure 4. The spectral density $\rho(\omega)$ for various values of U for the whole energy regime (left) and the region in the gap (right); $\Delta_{sc} = 0.02$ and $\pi\Gamma = 0.2$.

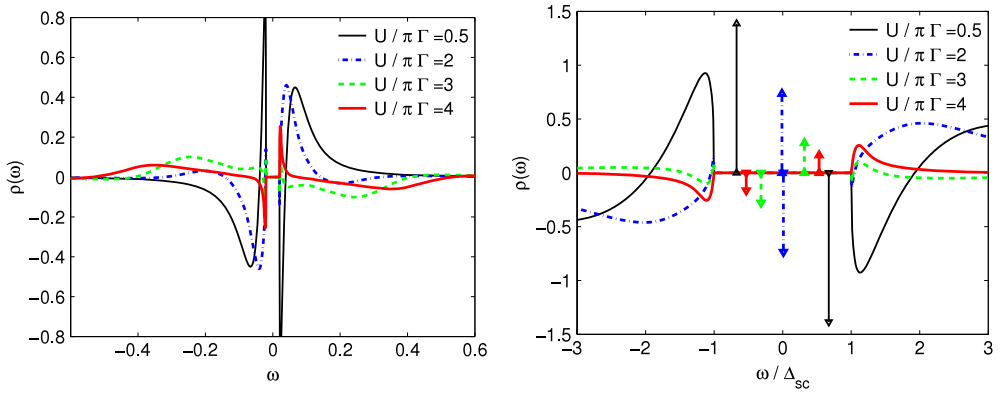

Figure 5. The spectral density $\rho^{\text{off}}(\omega)$ for various values of U for the whole energy regime (left) and the region in the gap (right); $\Delta_{sc} = 0.02$ and $\pi\Gamma = 0.2$.

For larger frequencies outside of the gap (left) we can see a peak near $\omega = \Delta_{sc}$, whose height is reduced on increasing U. At larger frequencies we find that the tails develop a broad peak for larger values of U. This has not been observed in the case with the smaller gap shown in figure 2. Also a sign change of the low energy peak is found as before. The behaviour near and in the gap (right) can be understood as before, where in this case we have shown two values of U with a singlet ground state and two with a doublet ground state.

3.1.4. Analysis of bound states with renormalized parameters. In section 2 we have discussed how the bound state energy, which so far was deduced from the spectral excitations (SE), can also be calculated from the bound state equation (BE) (8). The latter was derived by expanding the self-energy to first order. It involves the renormalized parameters $\tilde{\varepsilon}_d$, $\tilde{\Gamma}$ and the constant value of the off-diagonal self-energy $\Sigma^{\text{off}}(0)$. In figure 6 we compare the bound state energies calculated by these two methods for two values of the gap $\Delta_{sc} = 0.005$ (left) and $\Delta_{sc} = 0.06$ (right). We can see that for values of $U < U_c$ the agreement is excellent in both cases. However, when $U \geqslant U_c$ we find less accurate values with the method based on bound state equation (BE) with renormalized parameters. Since the method to calculate the bound state energy from the NRG spectral excitations (SE) is very accurate we expect inaccuracies to be found in the BE

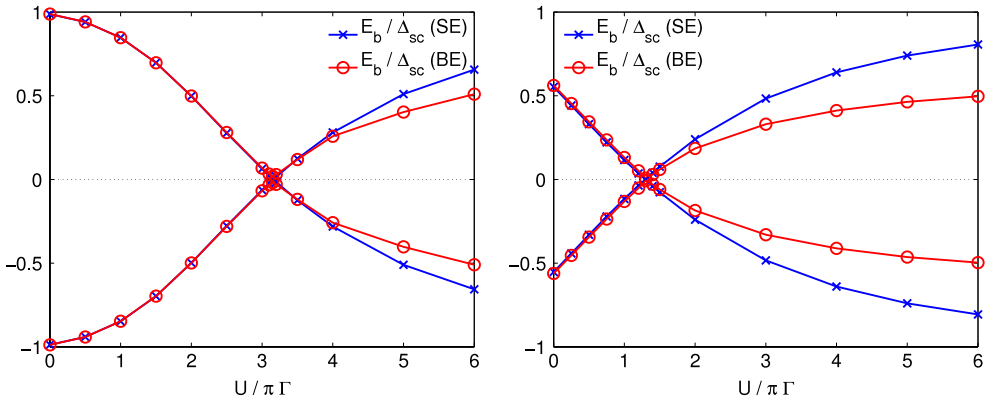

Figure 6. Bound state energies E_b as calculated from the spectral excitations (SE) and from the bound state equation (BE) (8) with renormalized parameters for $\Delta_{sc} = 0.005$ (left) and for $\Delta_{sc} = 0.06$ (right) for various $U/\pi\Gamma$; $\pi\Gamma = 0.2$ is fixed.

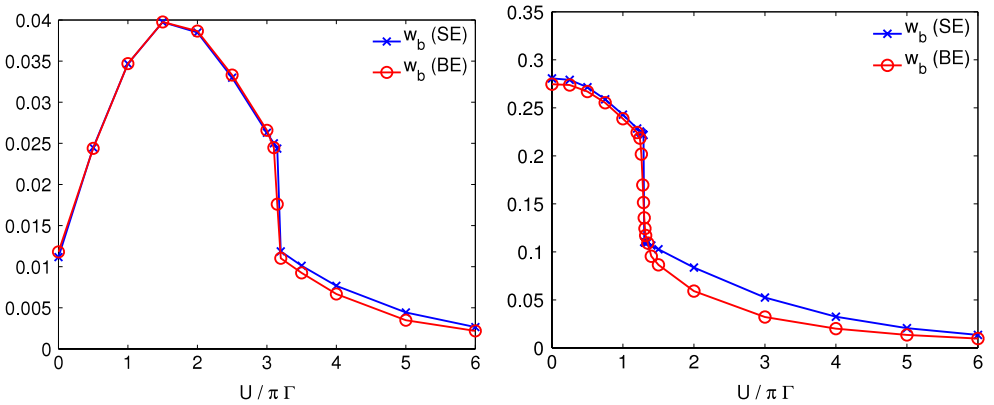

Figure 7. Weights w_b for the Andreev bound states as calculated from the spectral excitations (SE) and from the equation (11) with renormalized parameters for $\Delta_{sc} = 0.005$ (left) and for $\Delta_{sc} = 0.06$ (right) for various $U/\pi\Gamma$; $\pi\Gamma = 0.2$ is fixed.

method. Indeed, the closer inspection of the numerical results for the diagonal and off-diagonal self-energies reveals that the linear and constant approximation made in section 2.2 to derive the bound state equation with renormalized parameters (8) becomes less applicable for $U \geqslant U_c$. The self-energy displays additional features there.

In section 2 we have also derived an expression (11) for the weights w_b of the bound states in the gap. It can be expressed in terms of the renormalized parameters $\tilde{\varepsilon}_d$, $\tilde{\Gamma}$, the off-diagonal self-energy $\Sigma^{\text{off}}(0)$ and the bound states energy E_b. In figure 7 we compare the weights calculated from the spectral excitations (SE) with the ones from the bound state equation (BE) analysis with renormalized parameters. We show the results for the same parameters $\Delta_{sc} = 0.005$ (left) and $\Delta_{sc} = 0.06$ (right).

We can see for both cases that the overall behaviour of the weights as a function of U is described reasonably well by equation (11). It is, however, clearly visible that the agreement is between the SE and BE values is much better in the singlet regime for $U < U_c$. This is similar as observed for the values of the bound states energies E_b in figure 6, and the reason for this is the same. The discontinuity for the weight is not reproduced by the approximation

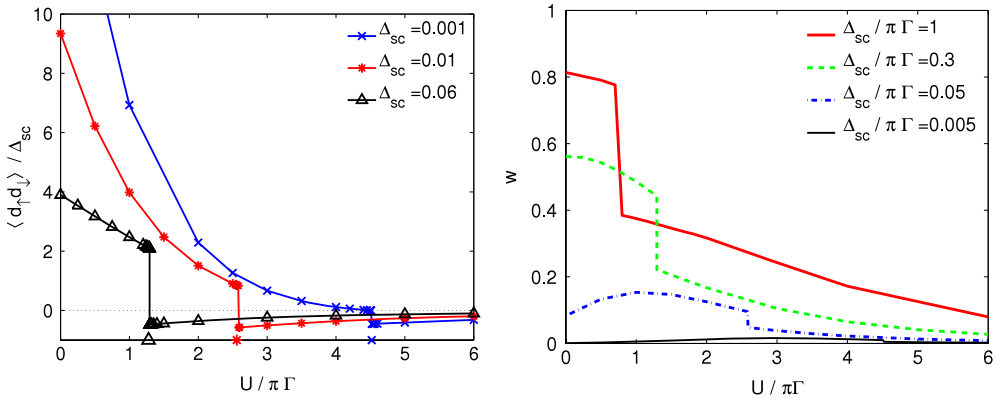

Figure 8. Left: anomalous expectation values $\langle d_\uparrow d_\downarrow \rangle$ as a function of $U/\pi\Gamma$ for various Δ_{sc}. The values are scaled by the gap Δ_{sc}; $\pi\Gamma = 0.2$. Right: the total weight of the bound states w in the gap as calculated from the spectral excitations as a function of $U/\pi\Gamma$ for various $\Delta_{sc}/\pi\Gamma$.

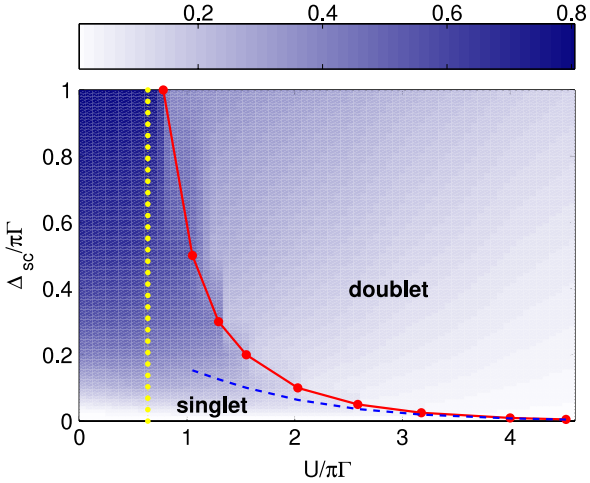

Figure 9. Phase diagram for singlet and doublet ground state as a function of $\Delta_{sc}/\pi\Gamma$ and $U/\pi\Gamma$, where the full line with large dots describes the phase boundary. The dotted line corresponds to $U/\Gamma = 2$, which shows the singlet doublet transition for $\Delta_{sc} \to \infty$. The dashed line gives the transition as $T_K/\Delta_{sc} \simeq 0.3$ with T_K given in equation (19). As a background colour we have included the amount of spectral weight transferred to the bound states; the discontinuous behaviour at the singlet doublet ground state transitions is slightly blurred in the interpolated representation.

based on equation (11). As can be seen from that equation this would require a sudden change in the self-energy as function of U, which was not found with sufficient accuracy in the present calculation. This can partly be attributed to the broadening procedure involved and to the inaccuracies when calculating the numerical derivative.

3.1.5. Anomalous expectation value and phase diagram. The anomalous expectation value $\langle d_\uparrow d_\downarrow \rangle$ is an indicator for the strength of the proximity effect of the superconducting medium at the impurity site and quantifies the induced on-site superconducting correlations. In the following figure 8 we show the dependence of $\langle d_\uparrow d_\downarrow \rangle$ on the interaction $U/\pi\Gamma$ for the same values of Δ_{sc} as in figure 3. The values are scaled by the gap Δ_{sc}.

We see that as a general trend $\langle d_\uparrow d_\downarrow \rangle$ decreases for increasing on-site interaction. This is expected since the superconducting correlations are suppressed by the repulsive interaction. We have marked the ground state transition with a symbol on the x-axis, and we see that $\langle d_\uparrow d_\downarrow \rangle$ changes discontinuously in magnitude and sign there. This is characteristic for this zero temperature quantum phase transition. The sign change is due to a phase change of π of the local order parameter which occurs at the transition as discussed in [11]. In the situation of infinite gap in the medium, which was discussed in section 2.3, $\langle d_\uparrow d_\downarrow \rangle$ drops only to zero at the transition point and is zero in the doublet ground state. At finite temperature the behaviour becomes continuous.

An overview of the transfer of spectral weight from the continuum to the bound states is shown in figure 8 (right). There we plot the total weight $w = w_b^+ + w_b^-$ as a function of $U/\pi\Gamma$ for four selected values of $\Delta_{sc}/\pi\Gamma$ ranging from 0.005 to 1. The curves are similar as before in figure 3 and show the discontinuity at the ground state transition. Here the values are not scaled by Δ_{sc}. We can see that the smaller U and the larger Δ_{sc} are the more spectral weight is found in the bound states. In the extreme case of $\Delta_{sc} \to 0$ we have $w = 0$, and for large gap, $\Delta_{sc} \to \infty$, and small U equation (11) gives $w \to 1$. The tendency to both of these limiting cases can be inferred from figure 8 (right) and we can see that, for instance, for $\Delta_{sc} = \pi\Gamma$ already about 80% of the spectral weight is in the bound states.

Summarizing the behaviour for different parameters, we present a phase diagram for singlet and doublet states for the symmetric model in the following figure 9.

For small U the ground state is always a singlet. It can become a doublet when $U/\pi\Gamma$ is increased. The critical U_c for the transition decreases with increasing value of the gap Δ_{sc} as can be seen in the diagram. In the limit $\Delta_{sc} \to \infty$, the critical interaction is given by $U_c/\pi\Gamma = 2/\pi$, which is shown with a dotted vertical line in the figure. As mentioned in section 1 there have been estimates of the phase boundary for the singlet and doublet ground state in the strong coupling regime [13, 15] as $T_K/\Delta_{sc} \simeq 0.3$. In this case the Kondo temperature is given as in equation (3.9) in [15],

$$T_K = 0.182U\sqrt{\frac{8\Gamma}{\pi U}}\mathrm{e}^{-\pi U/8\Gamma}. \tag{19}$$

We have added a dashed line representing this result which agrees with the ones presented here in the strong coupling regime, but starts to deviate for smaller values of U. As a background colour we have included in figure 9 how much spectral weight w is transferred to the bound states. (The value of w is given by the colour bar on the top part of the figure.) As noted before in figure 8 (right) we can see generally that the weight is maximal in the region of large gap and small on-site repulsion U.

At $\Delta_{sc} \to 0$ the ground state is a singlet for any value of U as the Kondo effect always leads to a screened impurity spin in a singlet formation. For finite gap the nature of the singlet ground state can differ depending on the magnitude of U. It can be a singlet corresponding to an s-wave pair as in the wavefunction given in equation (13), which is a superposition of zero and double occupation. This is the natural singlet ground state for a BCS superconductor. In the strong coupling regime we can, however, also have a screened local spin, i.e. a Kondo singlet. The wavefunction has a different form then and consists rather of a singly occupied impurity state coupled to the spins of the medium as many-body state. In our NRG calculations it is not easy to distinguish clearly this different nature of the singlet ground states and draw a definite line to separate them. We can, however, get an indication for what is favoured from the two-particle response functions in the spin and in the charge channel. In figure 10 we show the imaginary part of the dynamic charge and spin susceptibility, $\chi_c(\omega)$ and $\chi_s(\omega)$, for $\Delta_{sc} = 0.005$ and a series of values for the interaction U.

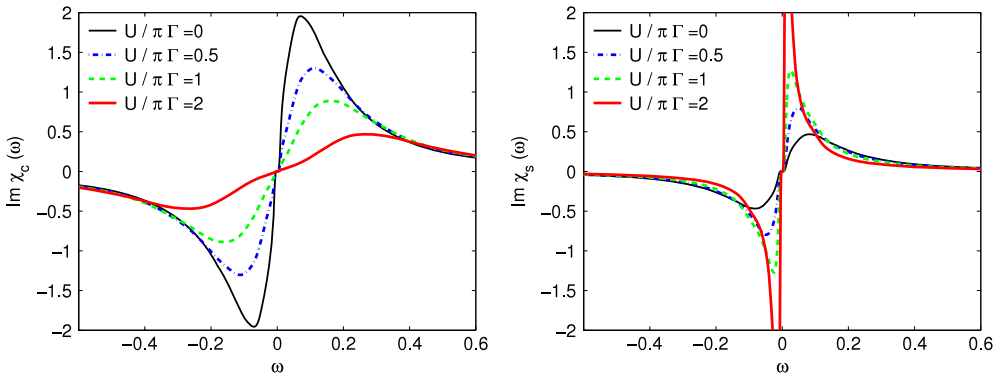

Figure 10. The imaginary part of the dynamic charge (left) and spin (right) susceptibility various values of U; $\Delta_{sc} = 0.005$ and $\pi\Gamma = 0.2$. The scale on both axes is the same such that the results can be compared well.

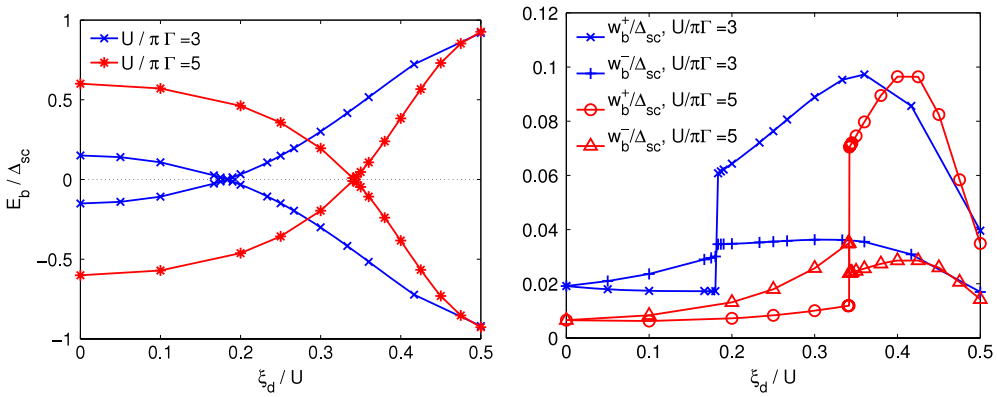

Figure 11. The dependence of the bound state energies E_b (left) and weights w_b (right) on ξ_d/U for $\Delta_{sc} = 0.01$ and $U/\pi\Gamma = 3, 5$; $\pi\Gamma = 0.2$ is fixed.

We can see that the peaks in the charge susceptibility exceed the ones in the spin susceptibility for zero and weak interaction indicating the dominance of the symmetry breaking in the charge channel, and a ground state of superconducting singlet nature. However, for $U/\pi\Gamma > 1$ the spin susceptibility develops a large and narrow peak at low frequency. This signals the importance of the spin fluctuations and low energy spin excitations and indicates ground states of a screened spin. In contrast the decreasing peaks in the charge susceptibility for large U is consistent with the effect of suppression of the on-site superconducting correlations.

3.2. Away from particle–hole symmetry

So far we have considered the special situation of particle–hole symmetry, $\varepsilon_d = -U/2$. In this section we will briefly discuss a few aspects that change in the situation away from particle–hole symmetry. Let us consider the case where for a given gap Δ_{sc}, on-site interaction U, and hybridization Γ, the ground state of the system is a doublet at half filling, $\xi_d = 0$. When ξ_d is increased, we find that a transition to a singlet state can occur at a certain value ξ_d^c. This is illustrated in the following figure 11, where we have plotted the bound state energy E_b for fixed

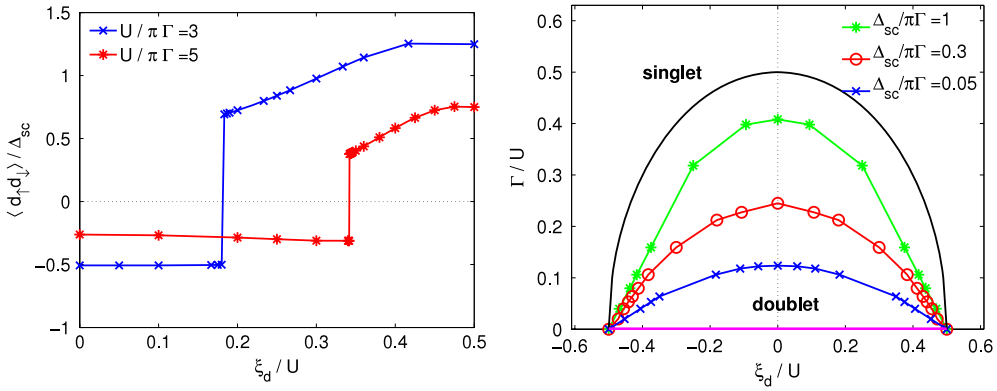

Figure 12. Left: anomalous expectation values $\langle d_\uparrow d_\downarrow \rangle$ for various $U/\pi\Gamma$, $\Delta_{sc} = 0.01$ and $\pi\Gamma = 0.2$. Right: phase diagram showing the regions for singlet and doublet ground state as dependent on Γ/U and ξ_d/U for different values of the gap Δ_{sc}. The full semicircular line corresponds to the phase boundary for $\Delta_{sc} = \infty$ as discussed in equation (15).

$\Delta_{sc} = 0.01$, two values of $U/\pi\Gamma = 3, 5$ and a series of values of the on-site energy scaled by U, ξ_d/U. As before we have $\pi\Gamma = 0.2$.

The critical interaction for the ground state transition for this case at half filling is $U_c/\pi\Gamma \simeq 2.6$, such that both cases possess a doublet ground state for $\xi_d = 0$. We can see that with increasing asymmetry ξ_d the bound state energy $|E_b|$ first decreases towards zero and then increases again in the singlet regime for $\xi_d > \xi_d^c$. As in the symmetric case the singlet–doublet transition is accompanied by $|E_b| = 0$. The weights $w_b^\pm$ for these bound states are shown on the right-hand side of figure 11. Away from particle–hole symmetry the weight w_b^+ for the positive energy E_b^+ and w_b^- the one for the negative bound state E_b^- are not equal, as was already pointed out below equation (11). We can see that the weights $w_b^\pm$ start to assume different values when ξ_d is increased from 0. At the ground state transition the values change discontinuously similar as observed in the half filled case. If we follow both the positive weight w_b^+ and the negative w_b^- separately the weights cross at the transition point. If, however, we think of the bound states as crossing at zero $E_b = 0$, positive and negative weights exchanged at the transition point, i.e. $w_b \leftrightarrow w_b^-$, then the weights do not cross. The discontinuous behaviour remains, however. In the singlet phase there is a maximum for both the positive and the negative bound state weight, more pronounced for w_b^+.

Also in the asymmetric case it is possible to calculate the bound state position E_b from equation (9) and the weights from equation (11) employing the renormalized parameters. We do not show the plots here, but note that the results resemble figures 6 and 7 in the respect that they give good agreement in the singlet regime, but deviations for parameters where the ground state is a doublet.

In the following figure 12 (left) we show the dependence of the anomalous expectation value $\langle d_\uparrow d_\downarrow \rangle$ on the asymmetry scaled by the interaction ξ_d/U for the same value of Δ_{sc} as in figure 11. The values for $\langle d_\uparrow d_\downarrow \rangle$ are scaled by the gap Δ_{sc}. For the values of U shown, at half filling the system has a doublet ground state and $\langle d_\uparrow d_\downarrow \rangle$ is negative. First it does not vary much when ξ_d is increased, but at the transition to the singlet ground state we find, as in the half filled case, a jump to a positive value and $\langle d_\uparrow d_\downarrow \rangle$ increases to a saturation value on further increasing ξ_d. This value is smaller for larger U, similar to what has been found in the symmetric case.

On the right-hand side of figure 12 we present a global phase diagram of the parameter regimes for singlet and doublet ground states for the non-symmetric case. This representation in

the Γ/U–ξ_d/U-plane is motivated by the result for the phase boundary for the case $\Delta_{sc} \to \infty$ derived in section 2.3, equation (15). The semicircle corresponding to this case is shown in the figure together with the phase boundaries for some finite values of the gap Δ_{sc}. These are seen to have a similar form, but the boundary decreases to smaller values of Γ/U with $\Delta_{sc}/\pi\Gamma$. Note that the parameters on the line on the x-axis, to which the phase boundary contracts in the limit $\Gamma \to 0$ or $U \to \infty$, possess a doublet ground state for $|\xi_d|/U < 1/2$.

4. Conclusions

We have discussed and quantitatively analysed the different forms of behaviour that can occur for an interacting impurity site in a medium with off-diagonal symmetry breaking in the charge channel. This study is motivated by the experimental situations of impurities in superconductors and nanoscale quantum dot systems with superconducting leads. In the local spectral functions we found that the low energy spectrum is dominated by the superconducting gap, and we saw that the lowest excitations in these cases are Andreev bound states within the gap region. For higher energies the spectrum resembles the form usually found in a metallic bath with broadened atomic limit peaks for large $U/\pi\Gamma$. The formation of the Kondo resonance, whose width is proportional to T_K, is in direct competition with the superconducting spectral gap of magnitude Δ_{sc}. Therefore, depending on the ratio of these parameters a screened Kondo singlet or an unscreened local moment is observed.

The lowest spectral excitations, the Andreev bound states within the gap region, change position and weight according to the other parameters. These have been analysed in detail in both the symmetric and the asymmetric model. We have given a simple interpretation of their position and weight in terms of renormalized parameters. It turned out that the assumptions for the definition of these were satisfied better in the singlet ground state regime. The reason for this should be subject to further investigation. In the quantum dot systems currents have been observed involving multiple Andreev processes [19, 20]. It is expected that a quantitative understanding of these currents requires accurate information about the weight and position of the Andreev bound states, which have been provided here. To study the experimental situation in detail and to describe the differential conductance dependent on the local bound state behaviour can be subject of a separate publication, where also the details of the experimental set-up are taken into account more carefully.

The behaviour of the ground state of the system, which can be a spin singlet or a doublet, is summarized in the two phase diagrams in figures 9 and 12. For coinciding parameter ranges our results for the ground state and the locally excited states are in agreement with earlier NRG studies [13–15]. Differences can be seen in the spectral representation of the bound states in the gap. Here we report delta function peaks, whereas an earlier study [27] presented broadened peaks. The method of calculating spectral functions and the self-energy used and explained in the appendix of this paper will be relevant for extensions of the calculation to the lattice model within the dynamical mean field theory framework. There an effective Anderson impurity model could be used to study the phases with superconducting symmetry breaking, for instance, in the attractive Hubbard model.

Acknowledgments

We would like to acknowledge helpful discussions with R Bulla and Hyun-Jung Lee. JB is grateful for the hospitality at Osaka City University, where this work was initiated, and to SFB 484 at the University of Augsburg, where this work was finalized. JB thanks the Gottlieb

Daimler- and Karl Benz-Foundation, the Engineering and Physical Sciences Research Council (EPSRC), the German Academic Exchange Service (DAAD) and the Japan Society for the Promotion of Science (JSPS) for financial support, and AO acknowledges the support by the Grant-in-Aid for Scientific Research for JSPS. We also wish to thank W Koller and D Meyer for their earlier contributions to the NRG program.

Appendix A. Relevant Green's functions

For the Green's functions it is convenient to work in Nambu space, $\boldsymbol{C}_d^\dagger = (c_{d,\uparrow}^\dagger, c_{d,\downarrow})$, with 2×2 matrices. The relevant retarded Green's functions are then

$$\underline{G}_d(\omega) = \langle\langle \boldsymbol{C}_d; \boldsymbol{C}_d^\dagger \rangle\rangle_\omega = \begin{pmatrix} \langle\langle c_{d,\uparrow}; c_{d,\uparrow}^\dagger \rangle\rangle_\omega & \langle\langle c_{d,\uparrow}; c_{d,\downarrow} \rangle\rangle_\omega \\ \langle\langle c_{d,\downarrow}^\dagger; c_{d,\uparrow}^\dagger \rangle\rangle_\omega & \langle\langle c_{d,\downarrow}^\dagger; c_{d,\downarrow} \rangle\rangle_\omega \end{pmatrix} = \begin{pmatrix} G_{11}(\omega) & G_{12}(\omega) \\ G_{21}(\omega) & G_{22}(\omega) \end{pmatrix}. \tag{A.1}$$

In the NRG approach we calculate G_{11} and G_{21} directly and infer $G_{22}(\omega) = -G_{11}(-\omega)^*$, which follows from $G_{A,B}^{\mathrm{ret}}(\omega) = -G_{B,A}^{\mathrm{adv}}(-\omega)$ and $G_{A,B}^{\mathrm{ret/adv}}(\omega) = -G_{A^\dagger,B^\dagger}^{\mathrm{ret/adv}}(-\omega)^*$ for fermionic operators A, B. Similarly, we can find $G_{12}(\omega) = G_{21}(-\omega)^*$. In the derivation one has to be careful and include a sign change for up down spin interchange in the corresponding operator combination.

In the non-interacting case we can deduce the d-site Green's function matrix exactly. To do so rewrite the term H_{sc} by introducing the vector of operators and the symmetric matrix

$$\boldsymbol{C}_{\boldsymbol{k}} := \begin{pmatrix} c_{\boldsymbol{k},\uparrow} \\ c_{-\boldsymbol{k},\downarrow}^\dagger \end{pmatrix}, \qquad A_{\boldsymbol{k}} := \begin{pmatrix} \varepsilon_{\boldsymbol{k}} & -\Delta_{\mathrm{sc}} \\ -\Delta_{\mathrm{sc}} & -\varepsilon_{\boldsymbol{k}} \end{pmatrix}. \tag{A.2}$$

Then H_{sc} can be written as

$$H_{\mathrm{sc}} = \sum_{\boldsymbol{k}} \boldsymbol{C}_{\boldsymbol{k}}^\dagger A_{\boldsymbol{k}} \boldsymbol{C}_{\boldsymbol{k}}. \tag{A.3}$$

The matrix Green's function in the superconducting lead is then given by $\underline{g}_{\boldsymbol{k}}(\mathrm{i}\omega_n) = (\mathrm{i}\omega_n \mathbb{1}_2 - A_{\boldsymbol{k}})^{-1}$,

$$\underline{g}_{\boldsymbol{k}}(\mathrm{i}\omega_n)^{-1} = \mathrm{i}\omega_n \mathbb{1}_2 - \varepsilon_{\boldsymbol{k}}\tau_3 + \Delta_{\mathrm{sc}}\tau_1, \tag{A.4}$$

where τ_i are Pauli matrices. It follows that

$$\underline{g}_{\boldsymbol{k}}(\mathrm{i}\omega_n) = \frac{\mathrm{i}\omega_n \mathbb{1}_2 + \varepsilon_{\boldsymbol{k}}\tau_3 - \Delta_{\mathrm{sc}}\tau_1}{(\mathrm{i}\omega_n)^2 - (\varepsilon_{\boldsymbol{k}}^2 + \Delta_{\mathrm{sc}}^2)}. \tag{A.5}$$

From the equations of motion we find the expression for the free d-site Green's function as

$$\underline{G}_d^0(\mathrm{i}\omega_n)^{-1} = \mathrm{i}\omega_n \mathbb{1}_2 - \varepsilon_d\tau_3 - V^2\tau_3 \frac{1}{N}\sum_{\boldsymbol{k}} \underline{g}_{\boldsymbol{k}}(\mathrm{i}\omega_n)\tau_3. \tag{A.6}$$

In the wide band limit with a constant density of states the last term describing the hybridization of medium and impurity takes the form

$$-V^2 \frac{1}{N}\tau_3 \sum_{\boldsymbol{k}} \underline{g}_{\boldsymbol{k}}(\mathrm{i}\omega_n)\tau_3 = \Gamma \frac{\mathrm{i}\omega_n \mathbb{1}_2 + \Delta_{\mathrm{sc}}\tau_1}{E(\mathrm{i}\omega_n)}, \tag{A.7}$$

where $\Gamma = \pi V^2 \rho_{\mathrm{c}}$. We are mostly interested in the limit of zero temperature here, and the function in the denominator $E(z)$ after analytic continuation reads (ω real)

$$E(\omega) = \begin{cases} -\mathrm{i}\,\mathrm{sgn}(\omega)\sqrt{\omega^2 - \Delta_{\mathrm{sc}}^2} & \text{for } |\omega| > \Delta_{\mathrm{sc}} \\ \sqrt{\Delta_{\mathrm{sc}}^2 - \omega^2} & \text{for } |\omega| < \Delta_{\mathrm{sc}}. \end{cases} \tag{A.8}$$

In the non-interacting case for $T = 0$, we have therefore

$$\underline{G}_d^0(\omega)^{-1} = \omega \mathbb{1}_2 - \varepsilon_d\tau_3 + \Gamma \frac{\omega \mathbb{1}_2 + \Delta_{\mathrm{sc}}\tau_1}{E(\omega)}. \tag{A.9}$$

The Green's function is obtained by matrix inversion, which yields

$$\underline{G}_d^0(\omega) = \frac{1}{D(\omega)}\left[\omega\left(1+\frac{\Gamma}{E(\omega)}\right)\mathbb{1}_2 - \frac{\Gamma\Delta_{\rm sc}}{E(\omega)}\tau_1 + \varepsilon_d\tau_3\right], \tag{A.10}$$

where the determinant, $D(\omega) := \det(\underline{G}_d^0(\omega)^{-1})$ is given by

$$D(\omega) = \omega^2\left[1+\frac{\Gamma}{E(\omega)}\right]^2 - \frac{\Gamma^2\Delta_{\rm sc}^2}{E(\omega)^2} - \varepsilon_d^2. \tag{A.11}$$

The full Green's function matrix $\underline{G}_d(\omega)^{-1}$ at the impurity site is given by the Dyson matrix equation

$$\underline{G}_d(\omega)^{-1} = \underline{G}_0^{-1}(\omega) - \underline{\Sigma}(\omega), \tag{A.12}$$

where we have introduced the self-energy matrix $\underline{\Sigma}(\omega)$.

Appendix B. Self-energy using the higher F-Green's function

As described by Bulla *et al* [37] there is a method to calculate the self-energy employing a higher F-Green's function, and it can also be used for the case with superconducting bath. In order to derive the equations of motions for the correlation functions, the identity

$$\omega\langle\langle A; B\rangle\rangle_\omega + \langle\langle [H, A], B\rangle\rangle_\omega = \langle [A, B]_\eta\rangle \tag{B.1}$$

($\eta = +$ for fermions) is useful. The calculation taking into account all off-diagonal terms yields the following matrix equation

$$\underline{G}_0^{-1}(\omega)\underline{G}_d(\omega) - U\underline{F}(\omega) = \mathbb{1}_2, \tag{B.2}$$

with the matrix of higher Green's functions $\underline{F}(\omega)$,

$$\underline{F}(\omega) = \begin{pmatrix} F_{11}(\omega) & F_{12}(\omega) \\ F_{21}(\omega) & F_{22}(\omega) \end{pmatrix}. \tag{B.3}$$

We have introduced the matrix elements $F_{11}(\omega) = \langle\langle c_{d,\uparrow}n_\downarrow; c_{d,\uparrow}^\dagger\rangle\rangle_\omega$, $F_{12}(\omega) = \langle\langle c_{d,\uparrow}n_\downarrow; c_{d,\downarrow}\rangle\rangle_\omega$, $F_{21}(\omega) = -\langle\langle c_{d,\downarrow}^\dagger n_\uparrow; c_{d,\uparrow}^\dagger\rangle\rangle_\omega$ and $F_{22}(\omega) = -\langle\langle c_{d,\downarrow}^\dagger n_\uparrow; c_{d,\downarrow}\rangle\rangle_\omega$. In the NRG we calculate F_{11} and F_{21} and the others follow from $F_{12}(\omega) = -F_{21}(-\omega)^*$ and $F_{22}(\omega) = F_{11}(-\omega)^*$. We can define the self-energy matrix by

$$\underline{\Sigma}(\omega) = U\underline{F}(\omega)\underline{G}_d(\omega)^{-1}. \tag{B.4}$$

The properties of the Green's function and the higher F-Green's function lead to the relations $\Sigma_{12}(\omega) = \Sigma_{21}(-\omega)^*$ and $\Sigma_{22}(\omega) = -\Sigma_{11}(-\omega)^*$ for the self-energies. We can therefore calculate the diagonal self-energy $\Sigma(\omega) = \Sigma_{11}(\omega)$ and the off-diagonal self-energy $\Sigma^{\rm off}(\omega) = \Sigma_{21}(\omega)$ and deduce the other two matrix elements from them. With the relation (B.4) between $\underline{G}$, $\underline{F}$ and $\underline{\Sigma}$ the Dyson equation (A.12) is recovered from (B.2). Therefore, the Green's function can be calculated from the free Green's function as given in (A.10) and the self-energy as calculated from (B.4). This scheme is also useful for applications of dynamical mean field theory with superconducting symmetry breaking, where the self-energy matrix has to be calculated accurately to find a self-consistent solution.

References

[1] Bardeen J, Cooper L and Schrieffer J 1957 *Phys. Rev.* **108** 1175
[2] Cooper L 1956 *Phys. Rev.* **104** 1189
[3] Kondo J 1964 *Prog. Theor. Phys.* **32** 37
[4] Hewson A 1993 *The Kondo Problem to Heavy Fermions* (Cambridge: Cambridge University Press)
[5] Abrikosov A A and Gorkov L P 1961 *Sov. Phys.—JETP* **12** 1243
[6] Zittartz J and Müller-Hartmann E 1970 *Z. Phys.* **232** 11
[7] Zittartz J 1970 *Z. Phys.* **237** 419
[8] Müller-Hartmann E and Zittartz J 1971 *Phys. Rev. Lett.* **26** 428
[9] Shiba H 1973 *Prog. Theor. Phys.* **50** 50
[10] Matsuura T 1979 *Prog. Theor. Phys.* **57** 1823
[11] Balatsky A V, Vekhter I and Zhu J-X 2006 *Rev. Mod. Phys.* **78** 373
[12] Sachdev S 1999 *Quantum Phase Transitions* (Cambridge: Cambridge University Press)
[13] Satori K, Shiba H, Sakai O and Shimizu Y 1992 *J. Phys. Soc. Japan* **61** 3239
[14] Sakai O, Shimizu Y, Shiba H and Satori K 1993 *J. Phys. Soc. Japan* **62** 3181
[15] Yoshioka T and Ohashi Y 2000 *J. Phys. Soc. Japan* **69** 1812
[16] Goldhaber-Gordon D, Shtrikman H, Mahalu D, Abusch-Magder D, Meirav U and Kastner M A 1998 *Nature* **391** 156
[17] Cronenwett S M, Oosterkamp T H and Kouwenhoven L P 1998 *Science* **281** 540
[18] Ralph D C, Black C T and Tinkham M 1995 *Phys. Rev. Lett.* **74** 3241
[19] Buitelaar M R, Nussbaumer T and Schonenberger C 2002 *Phys. Rev. Lett.* **89** 256801
[20] Buitelaar M R, Belzig W, Nussbaumer T, Babić B, Bruder C and Schönenberger C 2003 *Phys. Rev. Lett.* **91** 057005
[21] Vecino E, Buitelaar M R and Yeyati A L 2004 *Solid State Commun.* **131** 625
[22] van Dam J A, Nazarov Y V, Bakkers E P A M, Franceschi S D and Kouwenhoven L P 2006 *Nature* **442** 667
[23] Rozhkov A V and Arovas D P 1999 *Phys. Rev. Lett.* **82** 2788
[24] Matsumoto D 2001 *J. Phys. Soc. Japan* **70** 492
[25] Vecino E, Martin-Rodero A and Yeyati A L 2003 *Phys. Rev.* B **68** 035105
[26] Siano F and Egger R 2004 *Phys. Rev. Lett.* **93** 047002
[27] Choi M-S, Lee M, Kang K and Belzig W 2004 *Phys. Rev.* B **70** 020502
[28] Oguri A, Tanaka Y and Hewson A C 2004 *J. Phys. Soc. Japan* **73** 2496
[29] Lihu S Y and Lei X L 2004 *Phys. Rev.* B **70** 205339
[30] Tanaka Y, Oguri A and Hewson A C 2007 *New J. Phys.* **9** 115
[31] Wilson K 1975 *Rev. Mod. Phys.* **47** 773
[32] Krishna-murthy H R, Wilkins J W and Wilson K G 1980 *Phys. Rev.* B **21** 1003
[33] Bulla R, Costi T and Pruschke T 2007 cond-mat/0701105 unpublished
[34] Peters R, Pruschke T and Anders F B 2006 *Phys. Rev.* B **74** 245114
[35] Weichselbaum A and von Delft J 2007 *Phys. Rev. Lett.* **99** 076402
[36] Anders F B and Schiller A 2005 *Phys. Rev. Lett.* **95** 196801
[37] Bulla R, Hewson A C and Pruschke T 1998 *J. Phys.: Condens. Matter* **10** 8365
[38] Yeyati A L, Martín-Rodero A and Vecino E 2003 *Phys. Rev. Lett.* **91** 266802
[39] Hewson A C 1993 *Phys. Rev. Lett.* **70** 4007
[40] Affleck I, Caux J-S and Zagoskin A M 2000 *Phys. Rev.* B **62** 1433